Hybrid Integral Equation/Monte Carlo Approach to Complexation Thermodynamics

K. Friedemann Schmidt[†] and Stefan M. Kast*

Institut für Physikalische Chemie, Technische Universität Darmstadt, Petersenstrasse 20, 64287 Darmstadt, Germany

Received: February 21, 2002; In Final Form: April 1, 2002

A new method for the rapid calculation of complexation free energy surfaces (FES) in solution is presented. The Monte Carlo (MC) simulation technique for solute−solute statistics is combined with the reference interaction site model (RISM) integral equation theory for solute−solvent and pure solvent statistics. Statistical-mechanical perturbation theory is used to determine complexation potentials of mean force and, from these, standard free energies of binding. The hybrid RISM/MC method is applied to calculate the selectivity of rigid 18-crown-6 for alkali metal ions in liquid methanol and acetonitrile. A full atom model of the host in its D_{3h} conformation is used for the calculations. The difference of binding free energies between the various ions is found to be in excellent agreement with the experimental data in the case of methanol, less accurate for acetonitrile. Additional information about the structure of the FES is extracted by scanning its topography. Two-dimensional slices through the FES are presented to illustrate the solvation structure of the complexes. By connecting local minima and saddle points, minimum energy pathways are revealed, leading to the globally optimal complex structure.

I. Introduction

The accurate calculation of free energies of complexation is one of the most challenging problems in the computational treatment of molecular recognition. Much effort has been spent during the past years to develop and improve microscopically detailed simulation techniques for the accurate calculation of binding affinities.[1] A general shortcoming of an atomistic treatment of the solvent phase is the large computational power needed for sufficient sampling of the solvent molecules, which motivated the development of approximate solvent models. Thermodynamic properties of solution systems can be computed quickly with sufficient accuracy by using approximate solvent models. Implicit models of the solvent simplify the molecular nature of the liquid by continuum properties such as the dielectric constant while the more detailed statistical solvent models replace the solvent by distribution functions that can be computed ahead of treating the solute degrees of freedom. A speedup of several orders of magnitude in computation time as compared to atomistic molecular dynamics or Monte Carlo (MC) simulations is therefore possible. Reference 2 gives a review of this topic.

The reference interaction site model (RISM) integral equations yield a statistical solvent model comprising a detailed description of the solvent structure depending on the conformation of solute molecules. Although the distribution functions are approximate, the structural results were shown to agree reasonably well for pure liquids,[3−5] and for solutions.[6−11] Since the free energy of solvation can be determined quickly from the solution of the integral equations the solvent-induced potential of mean force (PMF) for a given solute geometry is readily accessible. Further reduction to simpler intrasolute coordinates can be achieved by averaging over the resulting PMFs, usually by sampling intramolecular degrees of freedom from molecular simulations. This type of approach has been applied to polymer systems (PRISM/MC)[12,13] and to conformational MC sampling of single biomolecules.[14−16] In certain circumstances intrasolute correlation functions and, from these, the PMFs can be determined from a suitable integral equation alone: The PMFs for simple ions in solution have been calculated in the past by utilizing both the one-dimensional[17] (1D) as well as the three-dimensional[18,19] (3D) RISM approach (see also ref 20 and 21). Orientationally dependent PMFs of molecular ions in aqueous solution have been determined from the 3D-RISM approach.[22] This formally provides a route to free energies of binding via averaging over all orientations, but the computational effort is, however, large.

Although the shortcomings of the 1D-RISM treatment within the hypernetted chain (HNC) approximation as compared to the 3D case are well-known[23] (see also the molecule-site integral equation approach[24]) the former have a tremendous computational advantage when combined with a MC treatment of certain degrees of freedom, as will be shown later. The value of this procedure can be assessed by comparison with available experimental data. To this end, we present in this paper a method that combines MC sampling of the solute−solute configurational space for bimolecular association with the 1D-RISM equations within the HNC approximation, applied to the complexation of alkali metal ions and 18-crown-6 in methanol and acetonitrile. Several aspects of complexation will be discussed: 2D scans and minimum energy paths (MEP) of the free energy surface (FES) or multidimensional PMF reveal its topography and relevant mechanisms of binding in solution; free energy perturbation calculations yield effective 1D PMFs from which the free energy of complexation is determined. The article is outlined as follows: In the next section the hybrid MC/RISM approach is described. Section 3 provides computational details of the methods used. Our results are reported in section 4 and summarized in the final section.

* Corresponding author. Telephone: +49 6151 165397. Fax: +49 6151 164298. E-mail: kast@pc.chemie.tu-darmstadt.de.

[†] Present address: Aventis Pharma Deutschland GmbH., DI&A LG Informatics, Industriepark Höchst G838, 65926 Frankfurt, Germany.

10.1021/jp020495+ CCC: $22.00
Published on Web 05/25/2002

II. Theory

(a) RISM Equations and Free Energy Determination. The 1D-RISM equations, initially developed by Chandler and Andersen,[25] are nonlinear integral equations for the correlation functions of molecular liquids composed of sites α and γ taking the form

$$\mathbf{h}^{vv} = \boldsymbol{\omega}^{v} * \mathbf{c}^{vv} * (\boldsymbol{\omega}^{v} + \rho \mathbf{h}^{vv}) \tag{1}$$

$$\mathbf{h}^{Xv} = \boldsymbol{\omega}^{X} * \mathbf{c}^{Xv} * (\boldsymbol{\omega}^{v} + \rho \mathbf{h}^{vv}) \tag{2}$$

$$\mathbf{h}^{YX} = \boldsymbol{\omega}^{Y} * \mathbf{c}^{YX} * \boldsymbol{\omega}^{X} + \boldsymbol{\omega}^{Y} * \mathbf{c}^{Yv} * \rho \mathbf{h}^{Xv} \tag{3}$$

where $\mathbf{h} = (h_{\alpha\gamma}(r))$ is the matrix of the total correlation functions (the radial distribution function is $g = h + 1$), $\mathbf{c} = (c_{\alpha\gamma}(r))$ are the direct correlation functions, $\boldsymbol{\omega} = (\omega_{\alpha\gamma}(r))$ are the intramolecular correlation functions (for rigid molecules these are normalized Dirac delta functions constraining the site distance), ρ is the site density, r is the distance, and the asterisk denotes convolution. Here, eq 1 is valid for pure solvents (superscript v), eq 2 is the solute−solvent relation in the limit of infinite solute dilution (superscript X or Y), and eq 3 yields the correlation functions between two solutes X and Y. The integral equations must be supplied with a suitable closure relation. Various closures have been proposed,[26−28] among them, particularly for polar systems the HNC approximation,[29]

$$h_{\alpha\gamma} = \exp(-\beta u_{\alpha\gamma} + h_{\alpha\gamma} - c_{\alpha\gamma}) - 1 \tag{4}$$

provides the best approximation to the pair distribution functions. Here, $u_{\alpha\gamma}$ is the pair potential and $\beta = 1/kT$, where k is the Boltzmann constant and T is the absolute temperature. The coupled eqs 1−3 and 4 are solved iteratively. The pair potentials used in this work are the sum of a short-ranged Lennard-Jones term and a long-ranged Coulomb term

$$u_{\alpha\gamma} = u^{LJ}_{\alpha\gamma} + u^{C}_{\alpha\gamma} = 4\epsilon_{\alpha\gamma}\left[\left(\frac{\sigma_{\alpha\gamma}}{r_{\alpha\gamma}}\right)^{12} - \left(\frac{\sigma_{\alpha\gamma}}{r_{\alpha\gamma}}\right)^{6}\right] + \frac{q_\alpha q_\gamma}{r_{\alpha\gamma}} \tag{5}$$

where q_i is the partial atomic charge on site i. For the Lennard-Jones parameters $\epsilon_{\alpha\gamma}$ and $\sigma_{\alpha\gamma}$, the standard Lorentz−Berthelot mixing rules are used. To ensure dielectric consistency at least on the level of a phenomenological dielectric constant, for the calculation of the pure solvent correlation functions, the solvent site charges are scaled so that the correct asymptotic behavior of the direct correlation functions is obtained.[17,30]

With a given set of HNC solute−solvent correlation functions, the excess chemical potential or transfer free energy from gas phase to solution is given in closed form as[31]

$$\Delta\mu = -\frac{\rho}{\beta}\sum_{\alpha,\gamma}\int \mathrm{d}\mathbf{r}\left(\frac{1}{2}h_{\alpha\gamma}{}^2 - c_{\alpha\gamma} + \frac{1}{2}h_{\alpha\gamma}c_{\alpha\gamma}\right) \tag{6}$$

Information about the solute−solute correlation can in principle be extracted from eq 3. As a matter of fact, a convergent solution of eq 3 for multisite molecules has not been reported in the literature, and we were not successful so far, either. Equation 3 has indeed been solved for pairs of monatomic solutes[17,20,21] only. The 3D generalization[22] of the solute−solute equation can be solved for fixed molecular orientations only. To overcome this problem with eq 3, a superposition approximation[32] was proposed where the PMF is assumed to be pair-decomposable, i.e., solute molecules are split into atomic sites, interatomic correlation functions are obtained from eq 3, and the full PMF is constructed according to a linear superposition of the site−site PMFs.

Although this approach has been successfully used in the construction of an intramolecular solvation FES,[33,34] we do not adopt the superposition approximation here. Instead, in this work a supermolecule XY comprising the complexation partners X and Y is constructed. Its conformation dependent solvent-induced part of the FES is in principle accessible by solving the RISM/HNC equations for each geometry and applying eq 6. Particularly when the resulting free energy is used in a molecular simulation with a statistical solvent model, the computational burden can be reduced drastically by applying a perturbation approximation that has first been derived by Archontis[35,36] (see also ref 37). We will derive it here in close analogy to the formulation of the RISM/HNC gradient as given by Sato et al.[38] Defining $t_{\alpha\gamma} = h_{\alpha\gamma} - c_{\alpha\gamma}$ the excess chemical potential may be written as

$$\Delta\mu = -\frac{\rho}{\beta}\sum_{\alpha,\gamma}\int \mathrm{d}\mathbf{r}\left(\exp[-\beta u_{\alpha\gamma} + t_{\alpha\gamma}] - 1 - t_{\alpha\gamma} - h_{\alpha\gamma}t_{\alpha\gamma} + \frac{1}{2}h_{\alpha\gamma}{}^2\right) - \frac{1}{(2\pi)^3\beta}\times \int \mathrm{d}\mathbf{k}\left(-\sum_{\alpha,\gamma}\hat{c}_{\alpha\gamma}\rho\hat{h}_{\alpha\gamma} + \frac{1}{2}\sum_{\alpha,\alpha',\gamma,\gamma'}\hat{c}_{\alpha\gamma}\hat{c}_{\alpha'\gamma'}\hat{\omega}_{\alpha\alpha'}\hat{\chi}_{\gamma\gamma'}\right) \tag{7}$$

where the carets denote Fourier transforms and $\boldsymbol{\chi} = \boldsymbol{\omega} + \rho\mathbf{h}$ is the solvent susceptibility. Viewing this expression as a functional of all $t_{\alpha\gamma}$, $h_{\alpha\gamma}$, $c_{\alpha\gamma}$, and $\omega_{\alpha\gamma}$, the total variation yields

$$\delta\Delta\mu = -\frac{\rho}{\beta}\sum_{\alpha,\gamma}\int \mathrm{d}\mathbf{r}\,[\{\exp[-\beta u_{\alpha\gamma} + t_{\alpha\gamma}] - 1 - h_{\alpha\gamma}\}\delta t_{\alpha\gamma} + \{-t_{\alpha\gamma} + h_{\alpha\gamma} - c_{\alpha\gamma}\}\delta t_{\alpha\gamma} + \{-h_{\alpha\gamma} + \rho^{-1}\sum_{\alpha',\gamma'}\omega_{\alpha\alpha'} * c_{\alpha'\gamma'} * \chi_{\gamma'\gamma}\}\delta c_{\alpha\gamma}] - \frac{1}{2(2\pi)^3\beta}\sum_{\alpha,\alpha',\gamma,\gamma'}\int \mathrm{d}\mathbf{k}\;\hat{c}_{\alpha\gamma}\hat{c}_{\alpha'\gamma'}\hat{\chi}_{\gamma\gamma'}\delta\hat{\omega}_{\alpha\alpha'} \tag{8}$$

For a convergent RISM/HNC solution the first three terms vanish as they represent the HNC closure, the definition of t, and the RISM equation, respectively.[31] Assuming negligible effects of a change of conformation on the direct correlation functions $c_{\alpha\gamma}$, the last term may be integrated functionally to give an incremental estimate of the change of the solvent-induced chemical potential upon moving from a geometry $\boldsymbol{\Gamma}$ to $\boldsymbol{\Gamma}'$ as

$$\Delta\mu(\boldsymbol{\Gamma}') - \Delta\mu(\boldsymbol{\Gamma}) \approx -\frac{1}{2(2\pi)^3\beta}\sum_{\alpha,\alpha',\gamma,\gamma'}\int \mathrm{d}\mathbf{k}\;\hat{c}_{\alpha\gamma}\hat{c}_{\alpha'\gamma'}\chi_{\gamma\gamma'}[\hat{\omega}_{\alpha\alpha'}(\boldsymbol{\Gamma}') - \hat{\omega}_{\alpha\alpha'}(\boldsymbol{\Gamma})] \tag{9}$$

With this equation, it is no longer necessary to recompute iteratively the RISM/HNC solution at every new geometry. Instead, eq 9 implies only simple matrix products and final integration. The quality of this approximation will be assessed for our case in section 3a.

(b) Binding Free Energy. The complexation thermodynamics is characterized by binding constants or, synonymously, the standard Gibbs free energy of binding

$$\Delta G^0_{XY} = \mu^0_{sol,XY} - \mu^0_{sol,X} - \mu^0_{sol,Y} \tag{10}$$

Its statistical-mechanical expression (see particularly Gilson et al.,[39] and also refs 40−42) is deduced from the chemical potential of a species i in its standard state in solution (at standard pressure $p^0 = 1$ bar and standard concentration $c^0 = N_A \cdot 1$ mol l^{-1} with N_A being Avogadro's number)

$$\mu^0_{\mathrm{sol},i} = -RT \ln\left(\frac{1}{V_{N,i}\, c^0} \frac{Q_{N,i}}{Q_{N,0}}\right) + p^0 \bar{V}_i \qquad (11)$$

where R is the gas constant, Q is the canonical partition function (volume V) for N solvent molecules with (subscript i) and without (subscript 0) a solute particle, and $\bar{V}_i = V_{N,i} - V_{N,0}$ in the thermodynamic limit becomes the partial molar volume of the solute at infinite dilution. For a purely classical system and unless flexible fragments of the molecules are rigidly linked together, the partition function factorizes into a momentum contribution that is immediately integrated and a configurational part. Establishing a molecular axis system allows, furthermore, for a separation of intramolecular degrees of freedom and external coordinates covering the center-of-mass motion and overall rotation. Integrating the latter variables yields $V_{N,i}$ for the translational part and for the orientation a factor of $\eta_i = 8\pi^2$ in general for nonlinear molecules with internal structure and $\eta_i = 1$ for structureless particles. We obtain finally

$$\mu^0_{\mathrm{sol},i} = -RT \ln\left(\frac{\eta_i}{c^0 \sigma_i} \frac{Z_{N,i}}{Z_{N,0}} \prod_{j=1}^{M_i} (2\pi m_{i,j} RT)^{3/2}\right) + p^0 \bar{V}_i \quad (12)$$

where M_i is the number of atomic sites, $m_{i,j}$ is the atomic mass of site j, and σ_i is the symmetry number of the solute. Z is the configuration integral; for the solute coordinates it is taken in the molecular frame. The ratio of configuration integrals can be further simplified by utilizing the excess chemical potential for a solute molecule in a specific conformation as

$$\frac{Z_{N,i}}{Z_{N,0}} \equiv Z_i = \int \mathrm{d}\mathbf{\Gamma} \exp\{-\beta[U_i(\mathbf{\Gamma}) + \Delta\mu_i(\mathbf{\Gamma})]\} \qquad (13)$$

where U_i is the total intramolecular potential of species i. Collecting all terms for the binding free energy the momentum contributions cancel and the final result is

$$\Delta G^0_{\mathrm{XY}} = -RT \ln\left(c^0 \frac{\eta_{\mathrm{XY}}}{\eta_{\mathrm{X}}\eta_{\mathrm{Y}}} \frac{\sigma_{\mathrm{X}}\sigma_{\mathrm{Y}}}{\sigma_{\mathrm{XY}}} \frac{Z_{\mathrm{XY}}}{Z_{\mathrm{X}} Z_{\mathrm{Y}}}\right) + p^0 \Delta \bar{V}_{\mathrm{XY}} \quad (14)$$

Turning now to our case of ion−crown ether interaction, there is no change in the rotational symmetry of the complex with respect to the unbound crown state,[43] leading to cancellation of the symmetry number term. Furthermore, the orientation factors cancel as well since one of the complex partners is a structureless ion. In this work the crown ether in its isolated form and as a complex fragment is treated as rigid. In this case (as long as no flexible fragments are linked rigidly) the integrand in eq 13 has to be multiplied by Dirac δ functions representative for the constraint variables. Setting the intramolecular potential of the isolated crown to zero, we therefore have for both complex partners X and Y

$$-RT \ln Z_{\mathrm{X/Y}} = \Delta\mu_{\mathrm{X/Y}} \qquad (15)$$

Since all external degrees of freedom have been accounted for in the derivation of eq 14, we are left with three internal variables for the complex configurations. We may take the spherical polar coordinates r, θ, φ specifying the single site solute position for instance with respect to the host center of mass. A FES is then defined in the space of the three coordinates as the PMF

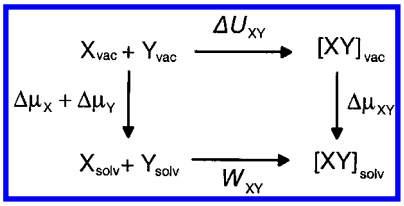

Figure 1. Thermodynamic cycle of the supramolecular approach for the determination of free energies of complexation in solution.

$$W(r,\theta,\varphi) = \Delta U_{\mathrm{XY}}(r,\theta,\varphi) + \Delta\mu_{\mathrm{XY}}(r,\theta,\varphi) - \Delta\mu_{\mathrm{X}} - \Delta\mu_{\mathrm{Y}} \qquad (16)$$

where ΔU_{XY} represents the vacuum solute−solute interaction energy. This may be understood as a thermodynamic cycle ansatz illustrated in Figure 1.

By neglecting the pressure−volume term, which is usually very small,[39] we obtain finally for our case from eqs 12−16

$$\Delta G^0_{\mathrm{XY}} = -RT \ln\{c^0 \int \mathrm{d}r\, \mathrm{d}\theta\, \mathrm{d}\varphi \sin\theta\, r^2 \exp[-\beta W(r,\theta,\varphi)]\} \qquad (17)$$

The integration boundaries depend on the geometrical definition of the complex as compared to isolated partners.[39] Up to this point the derivations given were formally exact for classical systems. The evaluation of the PMF needs the excess chemical potentials that are approximated in this work by the RISM/HNC theory.

(c) RISM/MC. From eqs 6, 10, and 16 the FES of the interaction of solvated rigid molecules can be determined. However, even if all intramolecular degrees of freedom are frozen, a computational scan of the FES is still expensive. On a rectangular grid of 40 Å with a spacing of 0.1 Å this requires approximately 10^8 evaluations. On the other hand, the calculation of 2D slices of the FES illustrating topographical features can be done quickly. For the purpose of determining the binding constant from evaluation of eq 17 it is advantageous to reduce the dimensionality by integrating over the angular variables with a special sampling procedure. In this way a one-dimensional PMF $w(r)$ is obtained. One could for instance use adaptive umbrella sampling,[44,45] possibly in conjunction with the weighted histogram analysis method (WHAM).[46,47] Alternatively, due to simplicity, we have implemented a MC procedure based on statistical-mechanical perturbation theory:[48−51] The PMF difference that results from a structural change is given by

$$w(r') - w(r) = -kT \ln\langle \exp\{\beta(W(r,\theta,\varphi) - W(r',\theta,\varphi))\}\rangle_r \qquad (18)$$

For our purposes, the average represents the sampling of angular coordinates with respect to a small change in the reaction coordinate r. Equation 18 gives only free energy differences between states r and r'. The PMF offset is calculated directly via eq 16 at such a large distance that the solvent-mediated interaction approaches zero.

A flowchart for the hybrid RISM/MC algorithm reads as follows:

I. Equations 1, 2, 4, and 6 are solved to yield free energies of solvation of the complex partners.

II. A supramolecular structure is constructed by placing X and Y at a large distance. Equations 2, 4, and 6 are solved to

TABLE 1: Force Field Parameters: Atomic Partial Charges q and Lennard-Jones Parameters σ and ϵ

site	q/e	σ/Å	ϵ/kcal mol^{-1}
methanol O	−0.7000	3.070	0.1700
methanol CH_3	0.2650	3.775	0.1180
methanol H	0.4350	0.400	0.0460
acetonitrile C	0.2800	3.650	0.1500
acetonitrile CH_3	0.1500	3.775	0.2070
acetonitrile N	−0.4300	3.200	0.1700
18-crown-6 C	0.1400	3.500	0.0660
18-crown-6 O	−0.4000	2.900	0.1400
18-crown-6 H	0.0300	2.500	0.0300
Na^+	1.0000	2.85	0.0314
K^+	1.0000	3.56	0.1304
Rb^+	1.0000	3.92	0.1530
Cs^+	1.0000	4.29	0.3594

obtain a set of reference distribution functions $\mathbf{h}_0$ and $\mathbf{c}_0$. The offset of the PMF is calculated.

III. A set of host−guest configurations is generated randomly by variation of the angular coordinates θ and φ. The PMF difference $W(r',\theta,\varphi) - W(r,\theta,\varphi)$ for a small step of the guest toward the host is calculated via eqs 9 and 16.

IV. Configurations are accepted with the probability P meeting the Metropolis criterion

$$P = \begin{cases} 1 & \leftrightarrow W(r,\theta,\varphi') \geq W(r,\theta,\varphi) \\ \exp\{\beta(W(r',\theta,\varphi) - W(r,\theta,\varphi))\} & \leftrightarrow W(r',\theta,\varphi) < W(r,\theta,\varphi) \end{cases} \quad (19)$$

V. The 1D PMF difference $w(r') - w(r)$ for a step of the guest toward the host is sampled according to eq 18.

Steps III−V are repeated until the reaction coordinate approaches zero.

The resulting 1D PMF contains the compressed information about the free energy surface from which the binding free energy is easily calculated. Equation 17 is recast as (see also Pranata and Jorgensen[50])

$$\Delta G^0_{XY} = -RT \ln\{4\pi c^0 \int_0^{r_c} dr\, r^2 \exp[-\beta w(r)]\} \quad (20)$$

All bound states are considered to contribute to the overall binding free energy, where the complex partners move within a contact distance in the first energy minimum. The integration therefore runs from zero to a certain cutoff distance r_c where the contact minimum ends. Contributions of complex partners moving along outer solvent-induced energy wells are neglected. For the sake of completeness we will also report results for a different standard concentration of 1 Å^{-3}, as these have been given in the literature as well.[51,52] These binding free energies will be termed ΔG_{XY} and differ from the correct standard free energies of binding by $\Delta G^0_{XY} - \Delta G_{XY} = 4.38$ kcal mol^{-1} at 298.15 K

(d) Computational Details. We used the *optimized potential for liquid simulation* (OPLS)[53,54] that has been extensively used for MC simulations of liquid systems.

The nonbonded interaction parameters for ions were taken from ref 55. OPLS provides three-site united-atom models for both methanol and acetonitrile. Geometric parameters as well as partial charges and Lennard-Jones parameters for acetonitrile and methanol were taken directly from OPLS with the exception of the hydoxyl H of methanol. To avoid Coulomb singularities that arise inevitably in the convolution of distribution functions when applied to nonrepulsive interaction sites, we set $\sigma_{HO} = 0.4$ Å and $\epsilon_{HO} = 0.046$ kcal mol^{-1}. The structure and nonbonded parameters of the crown ether in its D_{3h} symmetric conformation were also taken from the OPLS force field. The crown ether was kept rigid during the calculations. A complete overview of the nonbonded parameters used in this study is given in Table 1.

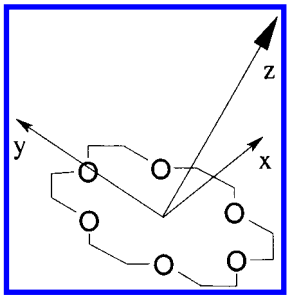

Figure 2. Coordinate system used for 18-crown-6. The ring plane of the crown is defined by the x and y axes.

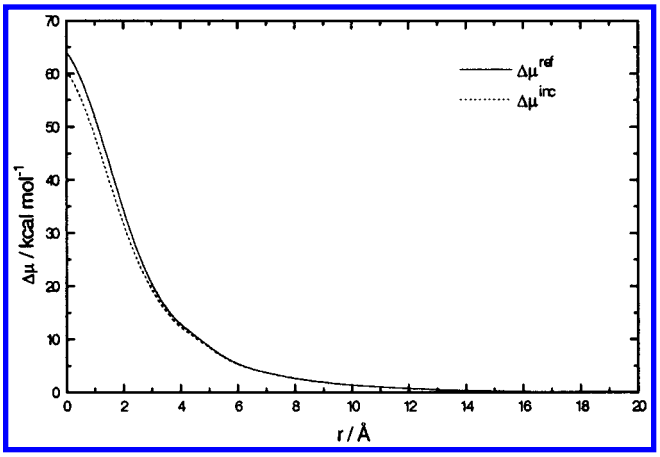

Figure 3. Exact RISM/HNC solvent-induced potential (solid) and approximate curve (dashed) from the incremental approximation eq 9 for the approach of a Na^+ ion toward the crown center along the z axis in methanol.

The RISM-HNC equations were solved on a logarithmically spaced grid of 512 points, ranging from a minimum of 5.98×10^{-3} Å to a maximum of 164.02 Å. For the calculation of fast Fourier transforms we used the Talman procedure.[56,57] Number densities of methanol and acetonitrile at 298.15 K were taken as 0.014 05 and 0.0116 Å^{-1}, as suggested for liquid-state simulations by Jorgensen.[58] The dielectric constants were set to 32.66 for methanol and 35.94 for acetonitrile. The solvent−solvent and solute−solvent integral equations were converged by iteratively improving the direct correlation functions until the threshold $\max(\Delta c_{\alpha\gamma}) < 10^{-5}$ was met (Picard method). For smooth convergence to the final solution, the potential was gradually increased and every new estimate of $\mathbf{c}$ was linearly mixed with the preceding iteration step.

III. Results

(a) Validation of the Incremental Approximation. The quality of eq 9 was assessed by comparing the solvent-induced chemical potential from explicit solution of the RISM/HNC equation with the approximate one for a certain pathway. We chose the approach of a Na^+ ion toward the crown center along the z axis in methanol. The crown ether coordinate system is defined in Figure 2.

The result is depicted in Figure 3. Note that for both curves the excess chemical potential at 20 Å distance was set to zero. This distance was also selected as the reference point for the

incremental formula, as used in the simulation and minimization work (see below).

As can be seen, the approximation is quite good throughout, the largest deviations are found near the crown center. This is not unexpected since in this region the local environment of the ion differs significantly from the reference state corresponding practically to infinite dilution. This effect has also been noted by Archontis[35] and is directly linked to a change of the direct correlation functions by burying sites that is neglected in applying eq 9. For our purposes, however, the approximation appears to be acceptable, particularly given the error already inherent to utilizing the RISM/HNC equations as an approximate solvation model.

(b) Structure of the FES. From the RISM solutions for alkali ions Na^+, K^+, Rb^+, Cs^+, and 18-crown-6 in methanol and acetonitrile the FES was constructed according to eqs 6, 9, and 16. Characteristics of the FES can be visualized by two-dimensional slicing planes defined in the crown ether coordinate system (Figure 2). A slice through the FES of the system 18-crown-6-ion in methanol is presented in Figure 4. The slicing plane is equal to the *xz* plane that is perpendicular to the ring plane of the crown.

In the case of K^+ and Na^+, a single contact minimum is found at the center of the crown, shielded by the crown's methylene groups. For Rb^+ and Cs^+, a strong barrier arises at the center of mass of the crown, prohibiting the passage of the ion through it. Approaching the center of mass of the crown, the ion must cross a region where the solvent shells of the host and the ion interfere. Oscillations are observed that depend strongly on the solute charges and the polarity of the solvent. In methanol, these oscillations are found to be of the order of 0.5 *kT*, while the local barriers in acetonitrile range from 1 to 2 *kT*. The largest barrier for the ions is found to be raised by the ether oxygens along the *z* axis of the crown near the center of mass. Local interference of the ions with solvent molecules interacting with the crown ether oxygens generates a barrier of approximately $1-2$ *kT*, which prevents a collinear attack of the ion in solution. This barrier is most probably due to an acetonitrile located along the *z* axis of the crown. The relatively low central barrier in methanol refers to laterally orientated solvent molecules.

(c) Potentials of Mean Force and Binding Free Energies. Radial PMFs were derived by the hybrid RISM/MC free energy perturbation method. The reaction coordinate was defined as the center of mass separation between the crown and the metal ion. The initial distance of the complex partners for the application of the incremental formula (eq 9) was chosen as 20 Å, ensuring independence of the PMF of the initial configuration. A total of 200 perturbation windows were sampled along the reaction coordinate, each with an offset of 0.1 Å. For each window, 10 000 solute configurations were sampled, yielding the average free energy difference for a 0.1 Å step of the ion toward the host. The results are depicted in Figure 5.

It is found that, depending on the size of the cation, the minima of the PMFs deviate significantly from the center of mass of the crown. They are found at 0.2, 1.0, 1.9, and 2.4 Å for Na^+, K^+, Rb^+, and Cs^+, respectively. In case of Na^+, which is smaller than the average cavity diameter of 5.6 Å, the ion prefers a slightly asymmetric position in the rigid crown that allows the ion to approach the three ether oxygens. In the case of the larger ions, we can attribute this behavior to the steric demand of the ion. A similar situation for the K^+ ion in water has been reported earlier.[59] The depth of the minima in methanol varies as $K^+ > Na^+ > Rb^+ > Cs^+$, while in case of acetonitrile, we find $Na^+ > K^+ > Rb^+ > Cs^+$.

Equation 20 was used to compute free energies of binding from the one-dimensional PMFs. A cutoff distance of 5 Å was used throughout; test calculations showed that for these systems all integrations converge after a few Å and do not change much upon variation of the cutoff distance. The experimental[60,61] and calculated free energies of binding are listed in Table 2a,b.

Looking first at the absolute standard free energies shows large discrepancies as compared to experiment, less so in the case of methanol as solvent. Apparently, the free energies without standard state correction match the experimental data better for methanol, which should be viewed as a mere coincidence. The relative free energy differences, however, show excellent agreement for complexation in methanol; in acetonitrile the trend is qualitatively correct except for sodium. The minima of the PMFs show basically the same trend and are useful at least for qualitative selectivity analysis. The difference between $\Delta\min(w(r))$ and $\Delta\Delta G°$ is related to the relative entropic contribution to the binding thermodynamics among the various ions: For instance, between Rb^+ and Cs^+ the entropic contribution changes less than between Na^+ and K^+.

The discrepancy between calculated and experimental absolute values originates from a variety of sources: The inherent deficiencies of the RISM/HNC theory, the use of the incremental free energy approximation, and inadequate models. Concerning the inaccuracy of eq 9, one could possibly do better by recomputing the RISM solutions at least for each new perturbation window. Using a rigid model for the crown ether is of course a crude approximation, we might expect that the resulting error will be different for different solvents. Acetonitrile as an aprotic solvent will most likely allow for stronger deformation of the crown upon complexation, particularly for small ions such as sodium. Also due to the aprotic property, the effect of counterions will be more pronounced as compared to methanol: If stable ion pairs exist on the reactant side, we would expect a large positive contribution to the binding free energy upon breaking up the pair. This might explain the large underestimation of absolute standard free energies for acetonitrile. In summary, if model deficiencies can be ruled out or safely ignored due to similar errors among a variety of reactants, the present method works well for selectivity analyses.

(d) Minimum Energy Path. Insight into reaction pathways and complexation mechanisms can be gained from local minimization of a number of configurations subject to a distance constraint. This has been done with an angular downhill simplex minimizer that does not require gradient information.[62] To ensure smoothness of the path, the choice of the constrained distances is critical. We used a 0.1 Å spacing, which is (see also Figure 4) considerably smaller than the average width of the solvent-induced barriers that are more than an order of magnitude larger than the spacing. Interconnections between these minimized points define the MEPs. This strategy allows for a graphical representation of valleys leading to the local minima of the FES and is exemplarily depicted for acetonitrile in Figure 6. The picture for methanol is qualitatively very close to that of acetonitrile, probably due to the similar dielectric solvent properties, and not shown here. Visualization was performed with the MOLCAD package.[63,64]

For the system K^+-18-crown-6 in aqueous solution, it has been stated that the ion's path approaching the host deviates strongly from the 3-fold crown symmetry axis.[59] For electrostatic reasons, this behavior might also be expected from the vacuum-PES of potassium-18-crown-6.[59,65] However, in both methanol and acetonitrile a collinear attack of the potassium ion is preferred up to a distance of approximately 5 Å only. Climbing

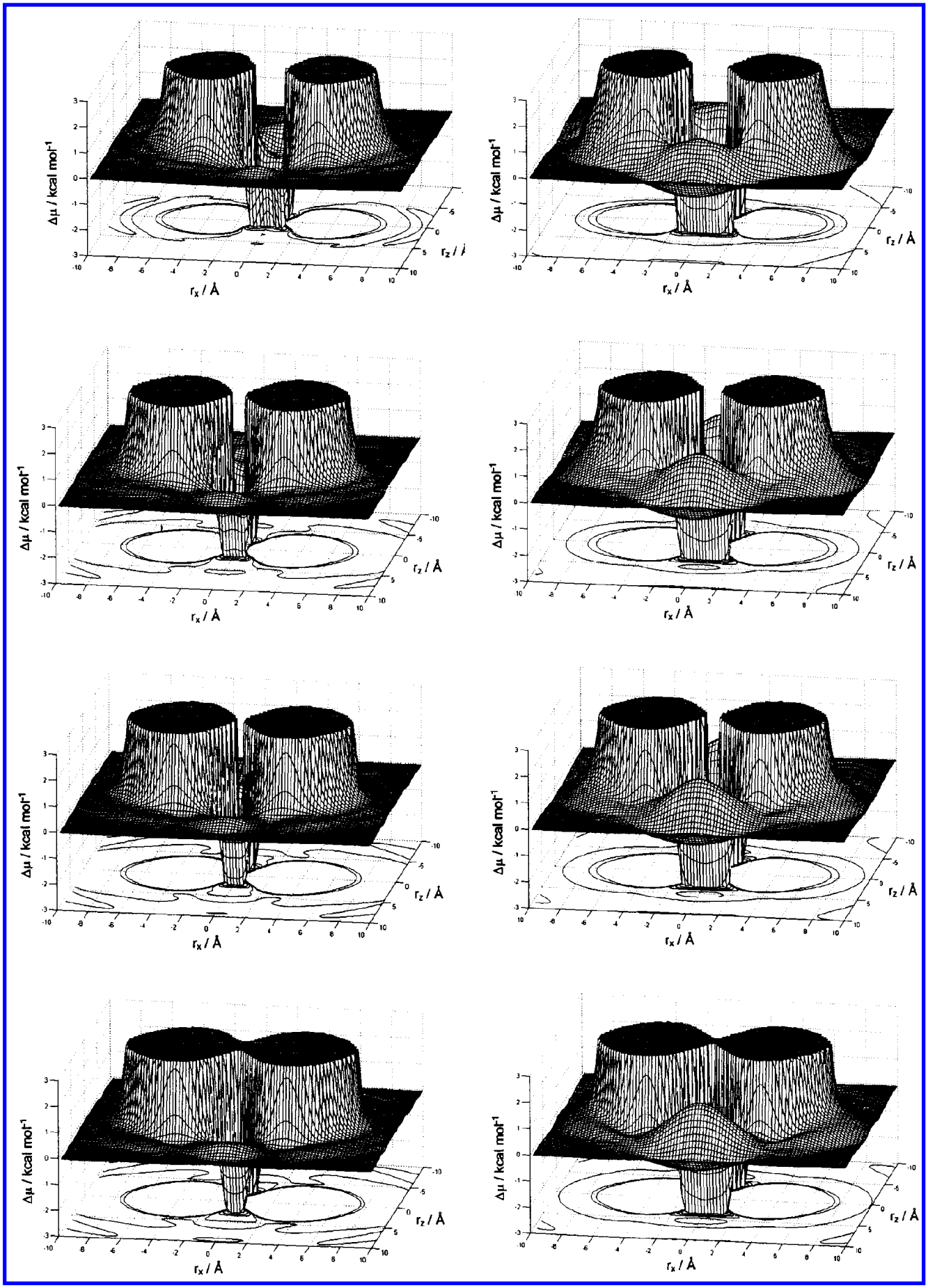

Figure 4. Slices through the FES of ion-18-crown-6 in methanol: (left) methanol, (right) acetonitrile; (from top to bottom) Na^+, K^+, Rb^+, Cs^+. The *z* axis and *x* axis of the crown ring as given in Figure 2 point toward the origin of the *x* axis and *z* axis, respectively.

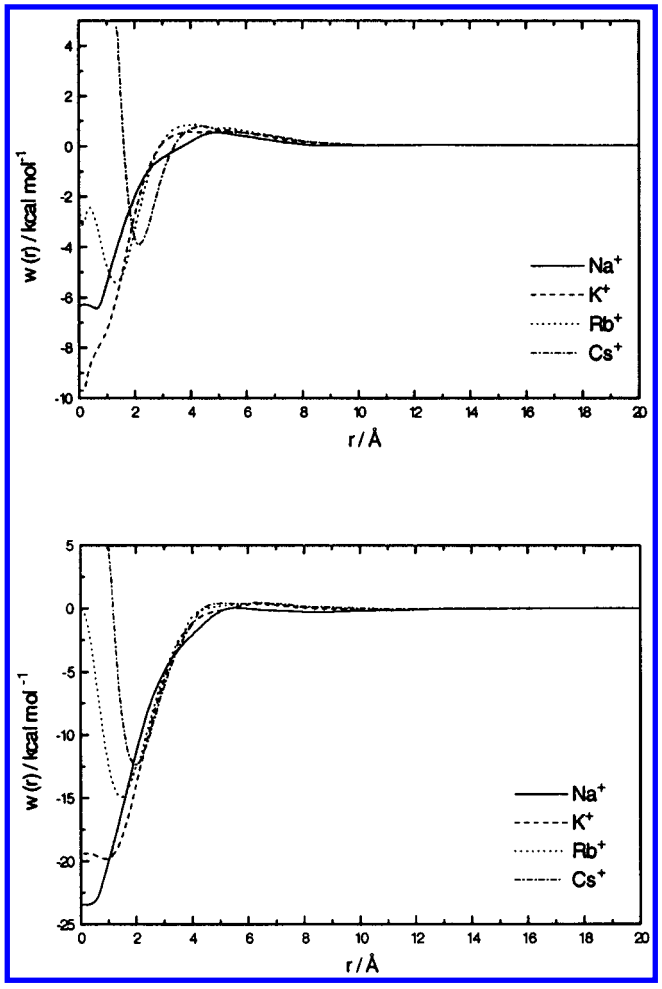

Figure 5. Orientationally averaged PMFs for the host−guest interaction: (top) in methanol; (bottom) in acetonitrile. The reaction coordinate is given by the distance between the crown center of mass and the ion.

TABLE 2: Free Energies of Complexation in Methanol andAcetonitrile, Relative Differences ($\Delta\Delta G$ and $\Delta\min(w)$) Refer to Adjacent Columns

a. In Methanol

ion	Na^+	K^+	Rb^+	Cs^+
contact minimum/Å	0.2	1.0	1.9	2.4
dissociative limit/Å	5.2	5.2	5.2	5.2
exptl $\Delta G°$/kcal mol^{-1}	-6.4 ± 1.0	-8.3 ± 0.2	-7.4 ± 0.4	-6.4 ± 0.2
calc $\Delta G°$/kcal mol^{-1}	−2.73	−4.70	−2.58	−1.54
exptl $\Delta\Delta G°$/kcal mol^{-1}		−1.9	0.9	1.0
calc $\Delta\Delta G°$/kcal mol^{-1}		−1.97	2.12	1.04
min($w(r)$)/kcal mol^{-1}	−6.29	−9.78	−5.42	−3.95
Δmin($w(r)$)/kcal mol^{-1}		−3.49	4.36	1.47
calc ΔG/kcal mol^{-1}	−7.11	−9.08	−6.96	−5.92

b. In Acetonitrile

ion	Na^+	K^+	Rb^+	Cs^+
contact minimum/Å	0.1	0.9	1.7	2.0
dissociative limit/Å	5.0	5.0	4.5	4.5
exptl $\Delta G°$/kcal mol^{-1}	-5.9 ± 0.8	-8.0 ± 0.5	-6.8 ± 0.4	-6.6 ± 0.2
calc $\Delta G°$/kcal mol^{-1}	−19.00	−16.67	−12.05	−9.81
exptl $\Delta\Delta G°$/kcal mol^{-1}		−2.1	1.2	0.2
calc $\Delta\Delta G°$/kcal mol^{-1}		2.33	4.62	2.24
min($w(r)$)/kcal mol^{-1}	−23.3	−19.9	−14.9	−12.4
Δmin($w(r)$)/kcal mol^{-1}		3.4	5.0	2.5
calc ΔG/kcal mol^{-1}	−23.38	−21.05	−16.43	−14.19

a small barrier, the ion is strongly attracted by a lateral oxygen. Therefore, it first moves to a lateral position near one ether oxygen, then proceeds directly to the 3-fold symmetry axis.

In summary, two main effects can be attributed to the solvent influence: (1) Due to necessary desolvation of both host and guest molecules the overall attraction of the complex partners is strongly screened. The depth of the minima is raised with respect to the vacuum potential.[59,65] (2) The interference of the solvent shells rises barriers between local minima (see also Figure 4). Such barriers are induced by solvent molecules "bridging" host and guest molecules and have been reported earlier for ion pair[20,21,66,67] and the system K^+-18-crown-6 in aqueous solution.[59]

Finally, Figure 7 shows the PMFs along the MEP in acetonitrile to get a clearer picture of the energetics.

It is interesting to note that the one-dimensional PMF (cf. Figure 5) is very similar to the MEP, more so for the lighter ions. We might conclude that the entropic contribution for movement orthogonal to the MEP is small and increases with the mass of the approaching ion.

IV. Conclusion

We have presented a hybrid RISM/MC technique specifically suited for rapid determination of free energy surfaces for bimolecular association in solution and applied it to study the complexation of alkali metal ions and 18-crown-6 in methanol and acetonitrile. The solute−solute configurational space can be explored with respect to various observables: Local minimization subject to a fixed distance constraint leads to the identification of minimum energy paths that are associated with the reaction mechanism in solution. Related information is gained from two-dimensional slices through the FES. By using the free energy perturbation method during sampling of the solute degrees of freedom, it is possible to construct a radially averaged potential of mean force from which the computation of the free energy of complexation is possible. The main computational advantage of our method stems from the incremental chemical potential approximation that relates a change of the solvent-induced-chemical potential to a change of conformation starting from one initial set of RISM solutions. It is therefore not necessary to recompute the explicit RISM solution for every new configuration, thus accelerating the computations substantially.

Interesting features of the FES were revealed by determination of minimum energy paths: Pathways with 3-fold symmetry leading to the global minimum were found that favor a lateral attack of the ions. Furthermore, a solvent-induced barrier shields a collinear attack. A similar structure of the FES of the system potassium-18-crown-6 in water has been proposed earlier. Although the 1D-RISM equations within the HNC approximation suffer from well-known limitations, the results obtained in this study compare reasonably well with experiment, notably better in the case of methanol. Within each series, the selectivity of the crown is found to be mostly consistent with the experimental data. The agreement is excellent at least in the case of methanol. Although the D_{3h}-symmetric geometry is the most stable conformation of 18-crown-6 in polar solvents, the rigidity of the model and, particularly in the acetonitrile case, the neglect of counterions probably accounts for a large part of the differences between the calculated and the experimentally measured free energies of complexation, Furthermore, the simplicity of the solvent models may pose problems.[68] We might conclude that 1D-RISM/HNC theory is well suited at least for the prediction of relative effects for similar complexes in solution. The transfer to other solvents requires a careful check of the models involved.

Ongoing work is concerned with the prediction of chiral selectivity in solution. The methods presented here will most

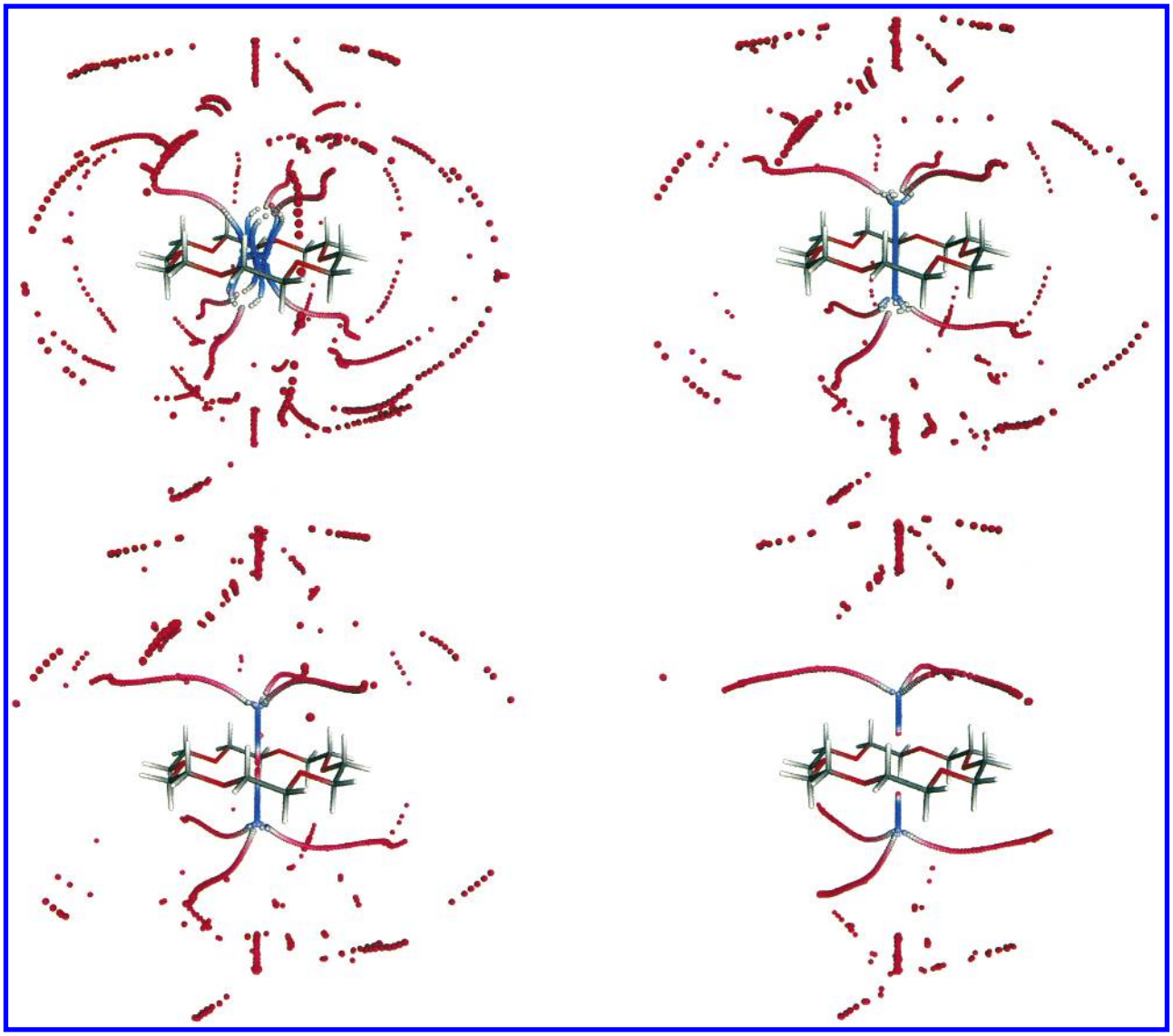

Figure 6. Color-coded minimum energy paths of Na^+, K^+, Rb^+, and Cs^+ (from top left to bottom right) approaching 18-crown-6 in acetonitrile. The scale ranges from blue (favorable) over white to red (unfavorable).

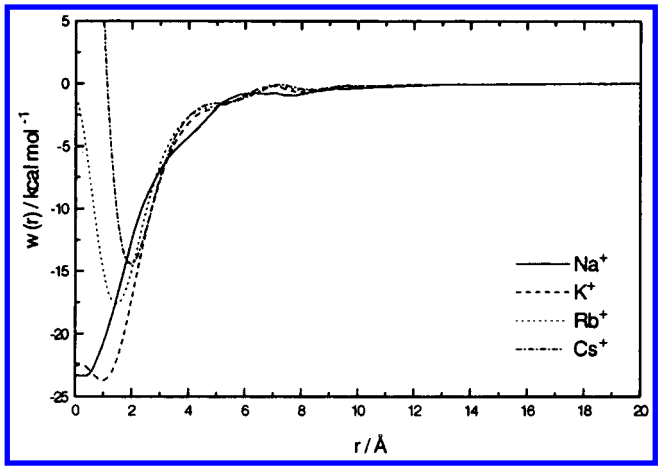

Figure 7. FES of host−guest interaction in acetonitrile along the minimum energy path.

likely be suited for this task that would need huge computational power if done with molecular simulation using explicit solvent models. For increasingly complex systems, more elaborate techniques of minimization on the FES will be needed.

Acknowledgment. Support of the VCI (Verband der Chemischen Industrie) and the Graduiertenkolleg der Deutschen Forschungsgemeinschaft "Kinetik von Ionenreaktionen in Lφsung" is gratefully acknowledged. We thank J. Brickmann and D. Zahn for stimulating discussions, M. Keil for support with new strategies of visualization, and an anonymous referee for referring us to G. Archontis who kindly provided excerpts of his work.

References and Notes

(1) Reddy, M. R.; Erion, M. D.; Agarval, A. In *Reviews in Computational Chemistry*; Lipkowitz, K. B., Boyd, D. B., Eds.; Wiley-VCH: New York, 2000; Vol. 16, p 217.
(2) Roux, B.; Simonson, T. *Biophys. Chem.* **1999**, *78*, 1.
(3) Hirata, F.; Rossky, P. J. *Chem. Phys. Lett.* **1981**, *83*, 329.
(4) Enciso, E. *Mol. Phys.* **1985**, *56* (1), 129.
(5) Kovalenko, A.; Ten-no, S.; Hirata, F. *J. Comput. Chem.* **1999**, *20*, 928.
(6) Chiles, R. A.; Rossky, P. J. *J. Am. Chem. Soc.* **1984**, *106*, 6867.
(7) Pettitt, M. B.; Karplus, M. *Chem. Phys. Lett.* **1987**, *136*, 383.
(8) Zichi, D. A.; Rossky, P. J. *J. Chem. Phys.* **1986**, *84*, 1712.
(9) Lee, P. H.; Maggiora, G. M. *J. Phys. Chem.* **1993**, *97*, 10175.
(10) Svensson, B.; Woodward, C. E. *J. Phys. Chem.* **1995**, *99*, 1614.
(11) Kawata, M.; Ten-no, S.; Kato, S.; Hirata, F. *J. Phys. Chem.* **1996**, *100*, 1111.
(12) Melenkevitz, J.; Schweitzer, K. S.; Curro, J. G. *Macromolecules* **1993**, *26*, 6190.

(13) Khalatur, P. G.; Khokhlov, A. R. *Mol. Phys.* **1998**, *93*, 555.
(14) Kinoshita, M.; Okamoto, Y.; Hirata, F. *J. Am. Chem. Soc.* **1998**, *120*, 1855.
(15) Kinoshita, M.; Okamoto, Y.; Hirata, F. *J. Chem. Phys.* **1999**, *110*, 4090.
(16) Mitsutake, A.; Kinoshita, M.; Okamoto, Y.; Hirata, F. *Chem. Phys. Lett.* **2000**, *329*, 295.
(17) Pettitt, M. B.; Rossky, P. J. *J. Chem. Phys.* **1986**, *84*, 5836.
(18) Beglov, D.; Roux., B. *J. Phys. Chem. B* **1997**, *101*, 7821.
(19) Kovalenko, A.; Hirata., F. *Chem. Phys. Lett.* **1998**, *290*, 237.
(20) Kovalenko, A.; Hirata, F. *J. Chem. Phys.* **2000**, *112*, 10391.
(21) Kovalenko, A.; Hirata, F. *J. Chem. Phys.* **2000**, *112*, 10403.
(22) Kovalenko, A.; Hirata, F. *J. Phys. Chem. B* **1999**, *103*, 7942.
(23) Kovalenko, A.; Hirata, F. *J. Chem. Phys.* **2000**, *113*, 2793.
(24) Cortis, C. M.; Rossky, P. J.; Friesner, R. A. *J. Chem. Phys.* **1997**, *107*, 6400.
(25) Chandler, D.; Andersen, H. C. *J. Chem. Phys.* **1972**, *57*, 1930.
(26) Hansen, J. P.; McDonald, I. R. *Theory of Simple Liquids*; Academic Press: London, 1980.
(27) Eu, B. C.; Rah, K. *J. Chem. Phys.* **1999**, *111*, 3327.
(28) von Solms, N.; Chiew, Y. C. *J. Chem. Phys.* **1999**, *111*, 4839.
(29) Fries, P. H.; Patey, G. N. *J. Chem. Phys.* **1985**, *82*, 429.
(30) Rossky, P. J.; Pettitt, B. M.; Stell, G. *Mol. Phys.* **1983**, *50*, 1263.
(31) Singer, S. J.; Chandler, D. *Mol. Phys.* **1985**, *55*, 621.
(32) Pettitt, B. M.; Karplus, M.; Rossky, P. J. *J. Phys. Chem.* **1986**, *90*, 6335.
(33) Lau, W. F.; Pettitt, B. M. *Biopolymers* **1987**, *26*, 1817.
(34) Pettitt, B. M.; Karplus, M. *Chem. Phys. Lett.* **1985**, *121*, 194.
(35) Archontis, G. Ph.D. Thesis, Harvard University, 1994.
(36) Lazaridis, T.; Archontis, G.; Karplus, M. *Adv. Protein Chem.* **1995**, *47*, 231.
(37) CHARMM Documentation, NIH/DCRT Laboratory for Structural Biology; FDA/CBER/OVRR Biophysics Laboratory, The Scripps Research Institute.
(38) Sato, H.; Hirata, F.; Kato, S. *J. Chem. Phys.* **1996**, *105*, 1546.
(39) Gilson, M. K.; Given, J. A.; Bush, B. L.; McCammon, J. A. *Biophys. J.* **1997**, *72*, 1047.
(40) Steinberg, I. Z.; Scheraga, H. A. *J. Biol. Chem.* **1963**, *238*, 172.
(41) Hermans, J.; Wang, L. *J. Am. Chem. Soc.* **1997**, *119*, 2707.
(42) Luo, R.; Head, M. S.; Given, J. A.; Gilson, M. K. *Biophys. Chem.* **1999**, *78*, 183.
(43) Hill, T. L. *Statistical Thermodynamics*; Addison-Wesley Publishing: London, 1950.
(44) Mezei, M. *J. Comput. Phys.* **1987**, *68*, 237.
(45) Paine, G. H.; Scheraga, H. *Biopolymers* **1985**, *24*, 1391.
(46) Kumar, S.; Bouzida, D.; Swendsen, R. H., Kollman, P. A.; Rosenberg, J. M. *J. Comput. Chem.* **1992**, *13*, 1011.
(47) Bartels, C.; Karplus, M. *J. Comput. Chem.* **1997**, *18*, 1450.
(48) Kollman, P. *Chem. Rev.* **1993**, *93*, 2395.
(49) Prue, J. E. *J. Chem. Educ.* **1969**, *46*, 12.
(50) Pranata, J.; Jorgensen, W. L. *Tetrahedron* **1991**, *47*, 2491.
(51) Dang, L. X.; Kollman, P. A. *J. Am. Chem. Soc.* **1990**, *112*, 5716.
(52) Dang, L. X.; Kollman, P. A. *J. Phys. Chem.* **1995**, *99*, 55.
(53) Jorgensen, W. L. *J. Am. Chem. Soc.* **1988**, *110*, 1657.
(54) Jorgensen, W. L. *J. Am. Chem. Soc.* **1996**, *118*, 11225.
(55) Wipff, G.; Weiner, P.; Kollman, P. A. *J. Am. Chem. Soc.* **1982**, *104*, 3249.
(56) Talman, J. D. *J. Comput. Phys.* **1978**, *29*, 35.
(57) Rossky, P. J.; Friedman, H. L. *J. Chem. Phys.* **1980**, *72*, 5694.
(58) Jorgensen, W. L. *User's manual of BOSS, Version 4.1*; Department of Chemistry, Yale University: New Haven, CT, 1999.
(59) Kowall, T.; Geiger, A. *J. Phys. Chem.* **1995**, *99*, 5240.
(60) Izatt, R. M.; Bradshaw, J. S.; Nielsen, S. A.; Lamb, J. D.; Christensen, J. J. *Chem. Rev.* **1985**, *85*, 271.
(61) Izatt, R. M.; Pawlak, K.; Bradshaw, J. S.; Bruening, R. L. *Chem. Rev.* **1995**, *95*, 2529.
(62) Press: W. H.; Flannery, B. P.; Teukolsky, S. A.; Vettering, W. T. *Numerical Recipes in C*; Cambridge University Press: Cambridge, U.K., 1988.
(63) Brickmann, J.; Goetze, T.; Heiden, W.; Moeckel, G.; Reiling, S.; Vollhardt, H.; Zachmann, C. D. In *Data Visualization in Molecular Science—Tools for Insight and Innovation*; Bowie, J. E., Ed.; Addison-Wesley: Reading, MA, 1995.
(64) Brickmann, J.; Exner, T.; Keil, M.; Marhöfer, R.; Moeckel, G. In *The Encyclopedia of Computational Chemistry*; Schleyer, P. v. R., Allinger, N. L., Clark, T., Gasteiger, J., Kollman, P. A., Schaefer, H. F., III, Schreiner, P. R., Eds.; Wiley: Chichester, U.K., 1998.
(65) Wipff, G.; Weiner, P.; Kollman, P. A. *J. Am. Chem. Soc.* **1982**, *104*, 3249.
(66) Dang, L. X.; Pettitt, B. M. *J. Phys. Chem.* **1990**, *94*, 4303.
(67) Gao, J.; Boudon, S.; Wipff, G. *J. Am. Chem. Soc.* **1991**, *113*, 9610.
(68) Dang, X. D. *Chem. Phys. Lett.* **1994**, *227*, 211.